Astronomy & Astrophysics manuscript no. paper
April 27, 2023

My paper on the cosmic microwave background and formation of structures in our Universe

V. A. Vikenes[1]

Institute of Theoretical Astrophysics, University of Oslo, 0315 Oslo, Norway
e-mail: v.a.vikenes@astro.uio.no

April 27, 2023

ABSTRACT

The code for this project can be found on my GitHub repository: https://github.com/Vikenes/AST5220/

Key words. cosmic microwave background – large-scale structure of Universe

1. Introduction

Write an introduction here. Give context to the paper. Citations to relevant papers. You only need to do this in the end for the last milestone.

2. Milestone I

In this section we will examine the evolution of the Universe's uniform background. Our primary objective is to develop methods for computing the Hubble parameter and related time- and distance measures. These methods provide a first step towards further investigations and modelling of the early Universe. To compute the background cosmology, we will solve ordinary differential equations (ODEs) numerically, using cosmological parameters obtained from the Planck Collaboration (Planck Collaboration et al. 2020). The parameters we will use are listed in Eq. (A.1) in Appendix A. One crucial aspect in the process is validating our model. We will therefore develop some simple methods for comparing our result. This will mainly involve considering simplified cases where analytical solutions can be obtained.

Our primary focus in this section concerns methods where the cosmological parameters are given from the start. Another interesting aspect is to use data to constrain cosmological parameters. To do this, we will use data from supernova observations (Betoule et al. 2014), containing luminosity distance associated with different values of redshift. By employing the numerical methods we develop initially, we will try to estimate optimal values of three cosmological parameters, by implement a simple Markov chain Monte Carlo (MCMC) algorithm. The parameters we will be sampling are h, Ω_{m0} and Ω_{k0}. From these results, we will investigate confidence regions of Ω_{m0} and $\Omega_{\Lambda 0}$, and try to estimate a probability distribution function (PDF) for the Hubble parameter.

The code for this milestone can be found on my GitHub repository: https://github.com/Vikenes/AST5220/tree/main/projects/milestone1

2.1. Theory

2.1.1. Density parameters and Hubble factor

The Friedmann equation can be written in terms of density parameters, $\Omega_i \equiv \rho_i/\rho_c$, where $\rho_c \equiv 3H^2/8\pi G$ is the critical density. The density of a given species, i, evolves as (Dodelson 2020, Eq. (2.61))

$$\rho_i(t) \propto a(t)^{-3(1+w_i)}, \tag{1}$$

where we have assumed that the equation of state (EoS) parameter, $w_i \equiv P_i/\rho_i$ (Dodelson 2020, Eq. 2.60), is constant. P_i denotes the pressure of the species. We will limit ourselves to consider three types of species in this report: matter, radiation and dark energy. We will only consider baryons and cold dark matter (CDM) for the matter component, which we express as $\Omega_{m0} = \Omega_{b0} + \Omega_{\mathrm{CDM}0}$. The subscript 0 is used to refer to today's value. The radiation component we consider is $\Omega_{r0} = \Omega_{\gamma 0} + \Omega_{\nu 0}$, corresponding to photons and neutrinos, respectively. For the dark energy, we only have the cosmological constant $\Omega_{\Lambda 0}$.

Matter, radiation and dark energy have densities evolving according to Eq. (1) with $w_i = 0$, $1/3$ and -1, respectively. Neutrinos having $w = 1/3$ only holds since we will assume that the neutrinos are massless. Curvature can be described by $w_i = -1/3$, with $\Omega_{k0} \equiv -kc^2/H_0^2$. The parameter k represents the curvature of the Universe, where $k = 0$ corresponds to a flat Universe. With these parameters, the Friedmann Equation can be written as (Dodelson 2020, Eq. (3.14))

$$H = H_0 \sqrt{\Omega_{m0}a^{-3} + \Omega_{r0}a^{-4} + \Omega_{k0}a^{-2} + \Omega_{\Lambda 0}}, \tag{2}$$

where $H \equiv \dot{a}/a$ is the Hubble parameter, with the dot denoting a derivative with respect to cosmic time, t. For the radiation, $\Omega_{\gamma 0}$ and $\Omega_{\nu 0}$ follow from the temperature of the CMB today, $T_{\mathrm{CMB}0}$, and the effective number of massless neutrinos, N_{eff}. They are given by

$$\Omega_{\gamma 0} = 2 \cdot \frac{\pi^2}{30} \frac{(k_b T_{\mathrm{CMB}0})^4}{\hbar^3 c^5} \cdot \frac{8\pi G}{3H_0^2}, \tag{3}$$

$$\Omega_{\nu 0} = N_{\mathrm{eff}} \cdot \frac{7}{8} \cdot \left(\frac{4}{11}\right)^{4/3} \Omega_{\gamma 0}. \tag{4}$$

The value of $\Omega_{\Lambda 0}$ is fixed by the requirement that $H(a = 1) = H_0$, yielding

$$\Omega_{\Lambda 0} = 1 - (\Omega_{m0} + \Omega_{r0} + \Omega_{k0}). \tag{5}$$

We also introduce the scaled Hubble factor, $\mathcal{H} \equiv aH$. Rather than working with the scale factor, $a(t)$, we will mainly be working with the logarithm of the scale factor

$$x \equiv \ln a, \quad ' \equiv \frac{\mathrm{d}}{\mathrm{d}x}. \tag{6}$$

The resulting expression for $\mathcal{H}(x)$ is thus

$$\mathcal{H}(x) = H_0 \sqrt{\Omega_{m0} e^{-x} + \Omega_{r0} e^{-2x} + \Omega_{k0} + \Omega_{\Lambda 0} e^{2x}}. \tag{7}$$

This form of the Hubble factor is the one we will focus on for the majority of this report. In terms of $\mathcal{H}(x)$, the value of the density parameters can be obtained at any given x, with

$$\Omega_k(x) = \frac{\Omega_{k0}}{\mathcal{H}(x)^2/H_0^2}, \tag{8}$$

$$\Omega_m(x) = \frac{\Omega_{m0}}{e^x \mathcal{H}(x)^2/H_0^2}, \tag{9}$$

$$\Omega_r(x) = \frac{\Omega_{r0}}{e^{2x} \mathcal{H}(x)^2/H_0^2}, \tag{10}$$

$$\Omega_\Lambda(x) = \frac{\Omega_{\Lambda 0}}{e^{-2x} \mathcal{H}(x)^2/H_0^2}, \tag{11}$$

From these expressions, we can identify the epochs during which the Universe was dominated by an equal amount of matter and radiation, and by an equal amount of matter and dark energy. These epochs are defined by the time when $\Omega_m = \Omega_r$ and $\Omega_m = \Omega_\Lambda$, respectively, and are a valuable asset towards understanding the physics governing the evolution of the Universe. Another time of interest is the onset of acceleration, defined as the time when $\ddot{a} = 0$. In terms of $\mathcal{H}$ and x, this corresponds to

$$\ddot{a} = \frac{\mathrm{d}x}{\mathrm{d}t}\frac{\mathrm{d}\dot{a}}{\mathrm{d}x} = \frac{\mathrm{d}\ln a}{\mathrm{d}t}\frac{\mathrm{d}\mathcal{H}(x)}{\mathrm{d}x} = e^{-x}\mathcal{H}(x)\frac{\mathrm{d}\mathcal{H}(x)}{\mathrm{d}x}. \tag{12}$$

In Sect. 2.1.4 we will derive an expression for $\mathcal{H}'(x)$.

2.1.2. Conformal time

We now want to relate the Hubble factor to some time variables. The main one we will consider is the conformal time, η. It is a measure of the distance light has been able to travel since $t = 0$, where t is the cosmic time. Using its definition in terms of t (Dodelson 2020, Eq. (2.90)), we can express it in terms of x as

$$\eta = \int_0^t \frac{c\,\mathrm{d}t'}{a(t')} = \int_{-\infty}^{x'} \frac{c\,\mathrm{d}x'}{\mathcal{H}(x')}. \tag{13}$$

This leads us to the following differential equation that we will solve numerically

$$\frac{\mathrm{d}\eta}{\mathrm{d}x} = \frac{c}{\mathcal{H}(x)}. \tag{14}$$

The initial condition we have is $\eta(-\infty) = 0$. Noting from Eq. (7) that $\mathcal{H}(x) \to H_0\sqrt{\Omega_{r0}}e^{-x}$ as $x \to -\infty$, we get an analytical approximation for the initial condition of η at early times

$$\eta(x_{\mathrm{start}}) \approx \int_{-\infty}^{x_{\mathrm{start}}} \frac{c\,\mathrm{d}x'}{H_0\sqrt{\Omega_{r0}}} e^{x'} = \frac{c}{\mathcal{H}(x_{\mathrm{start}})}. \tag{15}$$

Note that $\eta(x)\mathcal{H}(x)/c \to 1$ at low x, which provides a natural way of validating our implementation.

For the cosmic time, t, starting from $H = \dot{a}/a$ and applying the chain rule yields the desired differential equation for $t(x)$, which we will solve numerically,

$$\frac{\mathrm{d}t}{\mathrm{d}x} = \frac{1}{H(x)}. \tag{16}$$

To get an initial condition for t, we consider the radiation dominating era, with the following integral expression

$$t(x) = \int_{-\infty}^{x} \frac{\mathrm{d}x'}{H(x')}. \tag{17}$$

Comparing with Eq. (15), we see that the two integrands only differ by a factor e^x. The initial condition for t is therefore easily seen to be

$$t(x_{\mathrm{start}}) = \frac{1}{2H(x_{\mathrm{start}})}. \tag{18}$$

2.1.3. Distance measures

The supernova data we will study has distances measured in terms of luminosity distance, d_L. Expressing it in terms of the angular distance, $d_A = ar$, it becomes

$$d_L(a) = \frac{d_A}{a^2} = \frac{r}{a} \implies d_L(x) = e^{-x} r. \tag{19}$$

Here, r represents the radial coordinate of the emitted photon. To get an expression for r, we consider a photon's line-element in spherical coordinates,

$$ds^2 = -c^2 dt^2 + a^2\left(\frac{dr^2}{1-kr^2} + r^2 d\theta^2 + r^2 \sin^2\theta d\phi^2\right). \tag{20}$$

For photons travelling radially towards us, we have $\mathrm{d}\theta = \mathrm{d}\phi = 0$. Since $ds^2 = 0$ for photons, integrating the line-element of a photon emitted at, (t, r), reaching an observer at $(t_0, 0)$, yields

$$\int_0^r \frac{\mathrm{d}r'}{\sqrt{1-kr'}} = \int_t^{t_0} \frac{c\,\mathrm{d}t}{a}. \tag{21}$$

The RHS of Eq. (21) is known as the co-moving distance, χ, which in terms of conformal time is given as

$$\chi = \int_t^{t_0} \frac{c\,\mathrm{d}t}{a} = \int_x^0 \frac{c\,\mathrm{d}x'}{\mathcal{H}(x')} = \eta(0) - \eta(x). \tag{22}$$

Solving Eq. (21) with respect to r, we get

$$r = \begin{cases} \chi \cdot \frac{\sin\left(\sqrt{|\Omega_{k0}|}H_0\chi/c\right)}{\left(\sqrt{|\Omega_{k0}|}H_0\chi/c\right)}, & \Omega_{k0} < 0, \\ \chi, & \Omega_{k0} = 0, \\ \chi \cdot \frac{\sinh\left(\sqrt{|\Omega_{k0}|}H_0\chi/c\right)}{\left(\sqrt{|\Omega_{k0}|}H_0\chi/c\right)}, & \Omega_{k0} > 0. \end{cases} \tag{23}$$

Eq. (19) can now be used to compute d_L, and the expression to use depends on the curvature.

2.1.4. Analytical solutions

In Sect. 2.1.2 we discussed how $\eta(x)$ can be used to test our implementation in the radiation dominating era. To test our solutions in other regimes, we will need the first and second derivative of $\mathcal{H}(x)$. To simplify the resulting expressions, we define the function, $g(x)$, as the derivative of the term inside the square root in Eq. (7), namely

$$g(x) \equiv -\Omega_{m0}e^{-x} - 2\Omega_{r0}e^{-2x} + 2\Omega_{\Lambda 0}e^{2x}. \tag{24}$$

The first two derivatives of $\mathcal{H}(x)$ are easily seen to be

$$\frac{\mathrm{d}\mathcal{H}(x)}{\mathrm{d}x} = \frac{H_0^2}{2\mathcal{H}(x)}g(x), \tag{25}$$

$$\frac{\mathrm{d}^2\mathcal{H}(x)}{\mathrm{d}x^2} = \frac{H_0^2}{2\mathcal{H}(x)}\left[g'(x) - \frac{1}{2}\left(\frac{H_0 g(x)}{\mathcal{H}(x)}\right)^2\right]. \tag{26}$$

Now we will consider the situation where the Universe is dominated by a single fluid with a constant EoS parameter, w. In that case we have $H(t)^2 \propto \rho_i(t)^2$ (Dodelson 2020, Eq. (3.13)). Using Eq. (1), the Hubble parameter expressed in terms of w_i becomes

$$H(t)^2 \propto a^{-3(1+w)} \implies \mathcal{H}(x) = c_1 e^{-\frac{3}{2}(1+w)x}, \tag{27}$$

where c_1 is some constant. The reason for doing this, is that both c_1 and the exponential factor drops out when we consider $\mathcal{H}'(x)/\mathcal{H}(x)$ and $\mathcal{H}''(x)/\mathcal{H}(x)$. For different values of w_i, $\mathcal{H}'(x)/\mathcal{H}(x)$ becomes

$$\frac{1}{\mathcal{H}(x)}\frac{\mathrm{d}\mathcal{H}}{\mathrm{d}x} = -\frac{1+3w}{2} = \begin{cases} -1, & w = 1/3, \\ -1/2, & w = 0, \\ 1, & w = -1. \end{cases} \tag{28}$$

Similarly, the expression for $\mathcal{H}''(x)/\mathcal{H}(x)$ becomes

$$\frac{1}{\mathcal{H}(x)^2}\frac{\mathrm{d}^2\mathcal{H}}{\mathrm{d}x^2} = \frac{(1+3w)^2}{2} = \begin{cases} 1, & w = 1/3 \\ 1/4, & w = 0 \\ 1, & w = -1 \end{cases} \tag{29}$$

Equations (28) and (29) offer a means to evaluate the accuracy of our numerical solution at different regimes. Each density parameter evolve differently with x, as seen from Eqs. (8)-(11). Certain ranges of x-values will therefore closely resemble a Universe that is dominated by a single fluid. By computing $\mathcal{H}$, $\mathcal{H}'$, and $\mathcal{H}''$, we can examine whether these quantities exhibit the expected behaviour. This allows us to assess the validity of our model and ensure that it is consistent with the underlying physical principles.

2.2. Implementation details

To solve the differential equations for η and t (Eq. (14) and (16)) we use the C++ library GSL Galassi (2009), and use their Runge-Kutta4 solver. From the solution we create a spline of the results for the given x domain we have considered.

We will consider three different ranges of x-values. For the initial testing, we will use $x \in [\ln 10^{-10}, 5]$. For fitting cosmological parameters to the supernova data, we will use $x \in [\ln 10^{-2}, 0]$. When we want to estimate important times during the cosmic evolution, we will consider $x \in [-10, 1]$, for increased resolution, as the result may vary by a noticeable amount between step sizes. In all cases, we use $N_x = 10^5$ number of points.

The cosmological parameters we consider assume $\Omega_{k0} = 0$. In Sect. 2.2.1 we discuss how we will use supernova data to estimate a value for Ω_{k0}. Curvature is therefore implemented in all the relevant methods, but we set $\Omega_{k0} = 0$ when we're not dealing with supernova fitting.

2.2.1. Supernova fitting and parameter sampling

The supernova data we will use contains $N = 31$ data points of luminosity distance, $d_L^{\mathrm{obs}}(z_i)$, with associated measurement errors, σ_i, at different redshifts, $z_i \in [0.01, 1.30]$. This corresponds to $x \sim [-9.95 \cdot 10^{-3}, -0.833]$. Using these measurements, we want to constrain the three-dimensional parameter space

$$C = \left\{\hat{h},\ \hat{\Omega}_{m0},\ \hat{\Omega}_{k0}\right\}, \tag{30}$$

where the hat is used to distinguish the estimated parameters from the fiducial ones. We use $\Omega_{b0} = 0.05$ for this analysis, so $\hat{\Omega}_{m0}$ enters via $\Omega_{\mathrm{CDM}0} = \hat{\Omega}_{m0} - \Omega_{b0}$. Additionally, the neutrinos are not relevant at the small scale considered here, and we therefore set $N_{\mathrm{eff}} = 0$ for this analysis.

We will assume that the measurements at different redshifts are normal distributed and uncorrelated. The likelihood function is then given by $L \propto e^{-\chi^2/2}$, where

$$\chi^2(C) = \sum_{i=1}^{N} \frac{[d_L(z_i, C) - d_L^{\mathrm{obs}}(z_i)]^2}{\sigma_i^2}, \tag{31}$$

is the function we want to minimize. To do this, we will sample parameter values randomly by a Markov chain Monte Carlo (MCMC) process. We also restrict the parameter space to sample, with the following limits:

$$\begin{aligned} 0.5 &< \hat{h} < 1.5, \\ 0 &< \hat{\Omega}_{m0} < 1, \\ -1 &< \hat{\Omega}_{k0} < 1. \end{aligned} \tag{32}$$

To generate a new sample, we update each parameter by generating a random number $P \sim \mathcal{N}(0, 1)$, and multiplying it by a step size. We will use step sizes of $\Delta\hat{h} = 0.007$, $\Delta\hat{\Omega}_{m0} = 0.05$, $\Delta\hat{\Omega}_{k0} = 0.05$. To determine whether a new configuration should be included in the sample we use the Metropolis algorithm, where we always accept a state if it yields a lower value of χ^2 compared to the previous state that was accepted. If the new value of χ^2 is greater than the old one, we accept it if the ratio of the likelihood functions $L(\chi^2_{\mathrm{new}})/L(\chi^2_{\mathrm{old}}) > p$, where $p \sim \mathcal{U}(0, 1)$. We continue drawing samples until we get a total of $\hat{n} = 10^4$ samples. For the samples generated, we omit the first 1000 samples of the chain from our analysis.

With our generated samples, we can use the best fit, χ^2_{min}, to find the 1σ and 2σ confidence regions. For the χ^2 distribution with 3 parameters, these regions are given by $\chi^2 - \chi^2_{\mathrm{min}} < 3.53$ and $\chi^2 - \chi^2_{\mathrm{min}} < 8.02$, respectively. We will plot the 1σ and 2σ constraint in the $(\Omega_{m0}, \Omega_{\Lambda 0})$ plane. Since $\Omega_{r0} < 10^{-4}$, $\Omega_{\Lambda 0}$ can be approximated well by $\Omega_{\Lambda 0} = 1 - \Omega_{m0}$. After that we will plot the posterior probability distribution function (PDF) for H_0.

To compare our fit with the Planck data, we will plot $d_L^{\mathrm{obs}}(z_i)$ together with $d_L^{\mathrm{fit}}(z)$ and $d_L^{\mathrm{Planck}}(z)$. We obtain the former by solving the background cosmology with h, Ω_{m0}, Ω_{k0} replaced by the configuration $\hat{h}$, $\hat{\Omega}_{m0}$, $\hat{\Omega}_{k0}$ that yielded the lowest value of χ^2.

2.3. Results

In this section we present the results from our numerical simulations. Most of our results concern the evolution of various parameters as a function of x. Whenever it's relevant for interpreting and understanding the plot, we mark the point where we have matter-radiation equality and matter-dark energy equality, corresponding to $\Omega_m = \Omega_r$ and $\Omega_m = \Omega_\Lambda$, respectively. These points can be seen directly in Fig. 5.

2.3.1. Analytical and numerical comparisons

The dimensionless quantity $\eta\mathcal{H}/c$ is shown in Fig. 1. At the lowest values of $x \lesssim -10$, we see that $\eta\mathcal{H}/c = 1$, as expected. Slightly before matter-radiation equality takes place, we see a slight increase towards higher x. As we approach higher x, Ω_Λ starts dominating, and the solution eventually diverges, as expected.

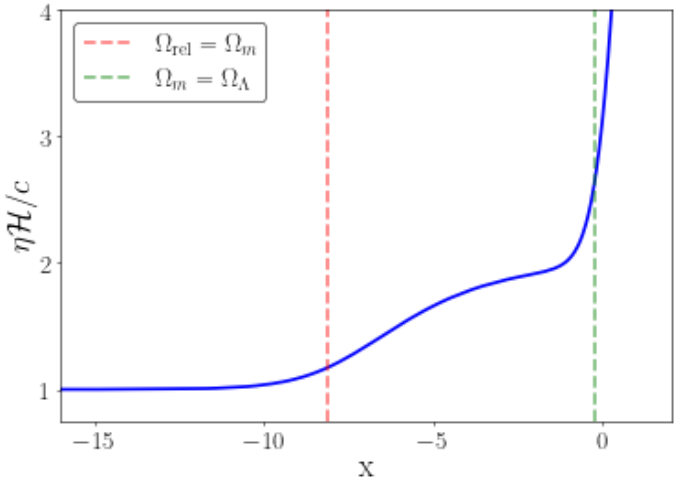

Fig. 1. The dimensionless quantity $\eta\mathcal{H}/c$ as a function of x. At low x it has a value of 1, as expected. The most significant changes occur near regions where there is a change in which density parameter is dominating.

In Fig. 2 we have plotted $\mathcal{H}'/\mathcal{H}$ and $\mathcal{H}''/\mathcal{H}$, where we include the analytical approximation from Eq. (28) and Eq. (29), respectively. The different values of w are drawn over the whole range of x where their related density parameter is larger than the other two. This is done for visibility purposes, and we only expect approximations to be reasonable whenever a density parameter is close to 1.

Towards the smallest values of x we see that both quantities are well approximated by the analytical solutions for $w = 1/3$. As we reach $x \gtrsim 12$, matter becomes increasingly dominant, and the solution deviates from being purely dominated by a $w = 1/3$ fluid. Towards the highest values of x, we see that both quantities reach a constant value of 1 for $w = -1$. At higher values of x, we know that both $\Omega_m(x)$ and $\Omega_r(x)$ should vanish, eventually, while $\Omega_\Lambda \to 1$. This behaviour is thus present in our implementation. When matter dominates, we see that both functions exhibit inferior agreement with the approximations compared to the other regimes. This can be understood from Fig. 5, where the vanishing contribution of Ω_r occurs around the same time as Ω_Λ starts contributing. The maximum value reached for this particular configuration is $\Omega_m \approx 0.995$. Nonetheless, significant deviations from the analytical solutions are not evident.

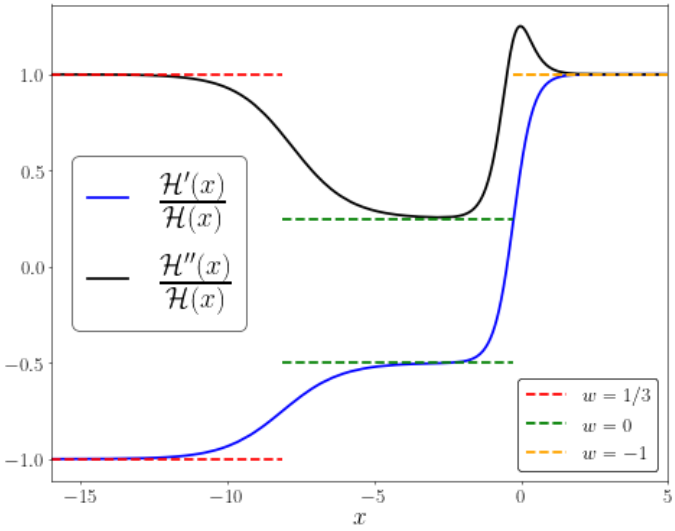

Fig. 2. $\mathcal{H}'/\mathcal{H}$ and $\mathcal{H}''/\mathcal{H}$ compared with analytical expressions in the case a single fluid with a given EoS parameter, w, shown by the dashed lines. The transition between the dashed lines are chosen as the corresponding epochs of equality.

2.3.2. Hubble factor and time variables

Having checked that our implementation is physical, we now proceed by studying the evolution of the background, starting with a plot of the conformal Hubble factor, $\mathcal{H}(x)$, show in Fig. 3.

The local minima taking place before matter-dark energy equality corresponds to the onset of acceleration, where $\ddot{a} = 0$. For $x > 0$, Ω_Λ will dominate the conformal Hubble factor, where we have $\mathcal{H}(x) \propto e^x$, as seen from Eq. (7).

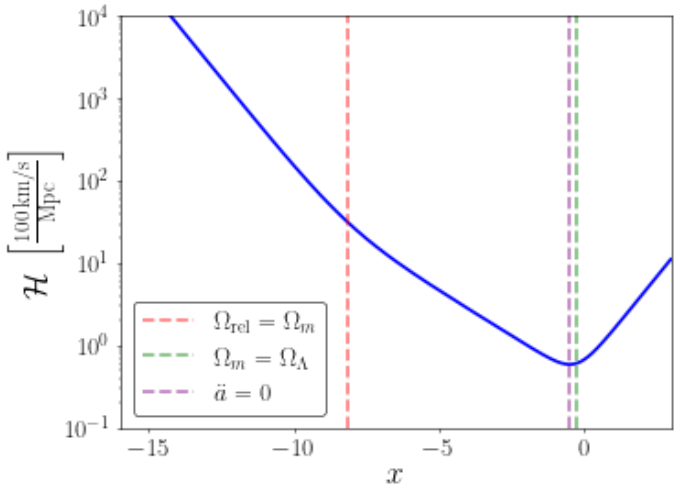

Fig. 3. Evolution of the conformal Hubble factor. The minimum point marks the onset of acceleration, after which, dark energy dominates its evolution.

The evolution of $\eta(x)$ and $t(x)$ is shown in Fig. 4. At high values of x, the e^x dependence of $\mathcal{H}(x)$ causes $\eta(x)$ to grow as e^{-x} at late times, suppressing its growth. The cosmic time, on the other hand, does not have an exponential dependence in the integrand at high values of x. This yields the linear growth we see at late times. The different x-dependece of t and η results in the two quantities to be approximately equal at $x \sim 2.75$.

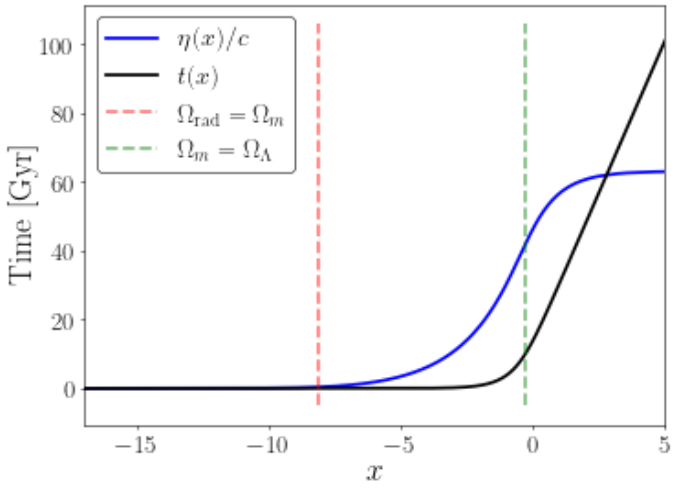

Fig. 4. The cosmic time, t and conformal time η/c. We emphasize that $\eta \neq t$ at small x, but the difference is discernable on the scale considered.

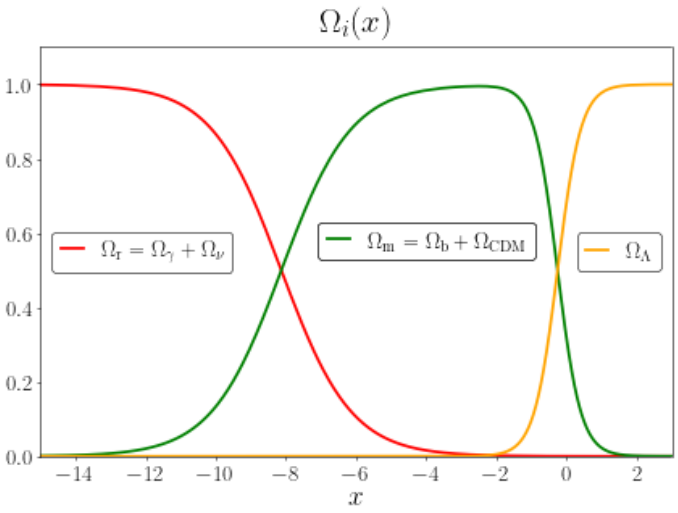

Fig. 5. Evolution of the density parameters over time. The points where $\Omega_m = \Omega_r$ marks the epoch of matter-radiation equality, and the intersection between Ω_m and Ω_Λ marks the epoch of matter-dark energy equality. The sum of the three quantities never exceed 1, as expected.

2.3.3. Supernova fitting

A plot showing the luminosity distance as a function of redshift is shown in Fig. 6, where we plot $d_L(z)/z$ to better compare the simulations with the data. There is a noticeable discrepancy between the simulated luminosity distance and the data, with most redshifts causing the simulation to fall outside the uncertainties.

The 1σ and 2σ confidence regions in the $\Omega_\Lambda - \Omega_m$ plane is shown in Fig. 7. In the figure we have also indicated the parameter configuration for a flat Universe. A majority of the configurations seem to favour a non-flat Universe, with $\Omega_{k0} \approx 0.0674$. This could be a result of local variations in the gravitational field at small scales.

The posterior PDF of H_0 is shown in Fig. 8, where we have included the resulting Gaussian distribution from the mean and variance of the sampled H_0 values. This shows further discrepancy from the value of $H_0 = 67\,\mathrm{km/s/Mpc}$, given by Planck, while the mean value we obtain is $\hat{H}_0 = 70.1\,\mathrm{km/s/Mpc}$, with a corresponding standard deviation of $\hat{\sigma}_{H_0} = 0.64\,\mathrm{km/s/Mpc}$.

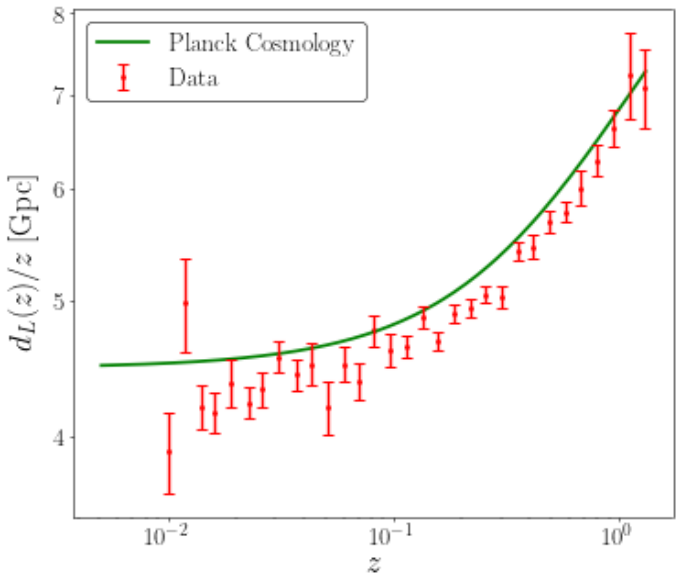

Fig. 6. Supernova data compared with the predicted luminosity distance obtained from simulations using Planck cosmology. Note that we use a logarithmic scale for the y-axis.

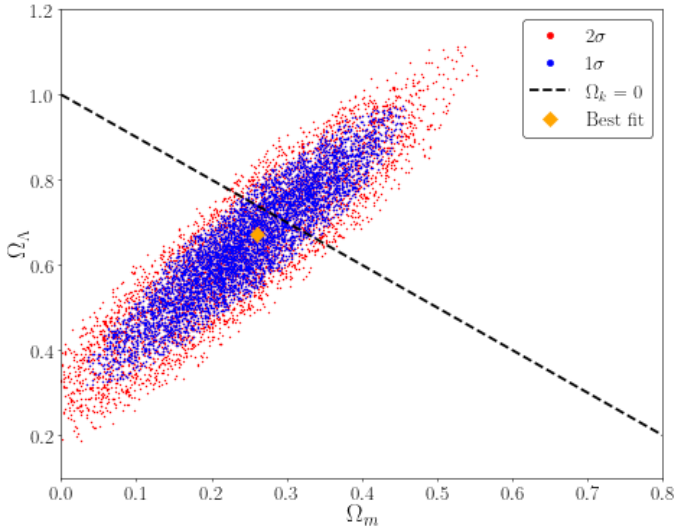

Fig. 7. Confidence regions of Ω_{m0} and $\Omega_{\Lambda 0}$ obtained from fitting the supernova data. The best fit parameter values are shown in the plot, as well as the configurations that would give a flat Universe.

With the fitted parameters, we can solve the background cosmology once again, and compute the resulting luminosity distance. The result is shown in Fig. 9, where the previous result from Fig. 6 is included for comparison purposes. The simulation with the best fit parameters yields a luminosity distance function that is much more consistent with data. However, there is still some discrepancy at lower redshift, but the associated data points in this regime have large uncertainties.

There are three important periods we have discussed, the times of matter-radiation equality, acceleration onset and matter-dark energy equality. The times when these incidents occur are listed in table 2.3.3, in terms of x, redshift z and cosmic time t. We also include the age of the Universe today, $t_0 \equiv t(x = 0)$, and the conformal time today, η_0/c.

	Matter-radiation equality $\Omega_m = \Omega_r$	Acceleration onset $\ddot{a} = 0$	Matter-dark energy equality $\Omega_m = \Omega_\Lambda$
x	-8.132	-0.487	-0.256
z	3400.460	0.627	0.291
t [Gyr]	$5.099 \cdot 10^{-5}$	7.750	10.372

Age of Universe today: $t_0 = 13.848$ Gyr

Conformal time today: $\eta_0/c = 46.284$ Gyr

Table 1. Important times during the evolution of the Universe, expressed in terms of x, redshift and cosmic time. In the last two rows we also present today's time values

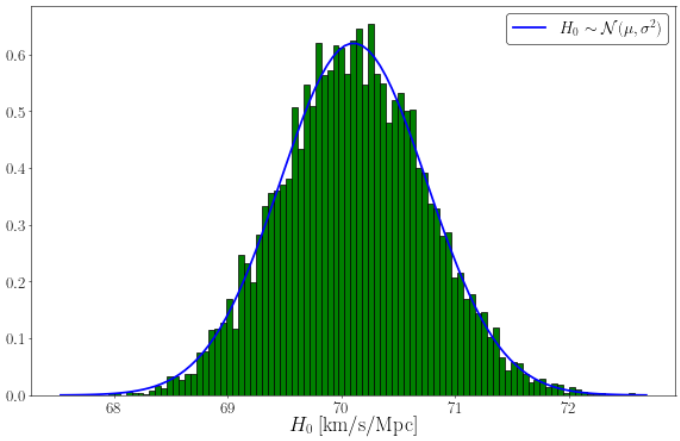

Fig. 8. Posterior PDF of H_0. The histogram shows the sampled values, while the blue curve is the corresponding normal distribution obtained from the mean and variance of the data.

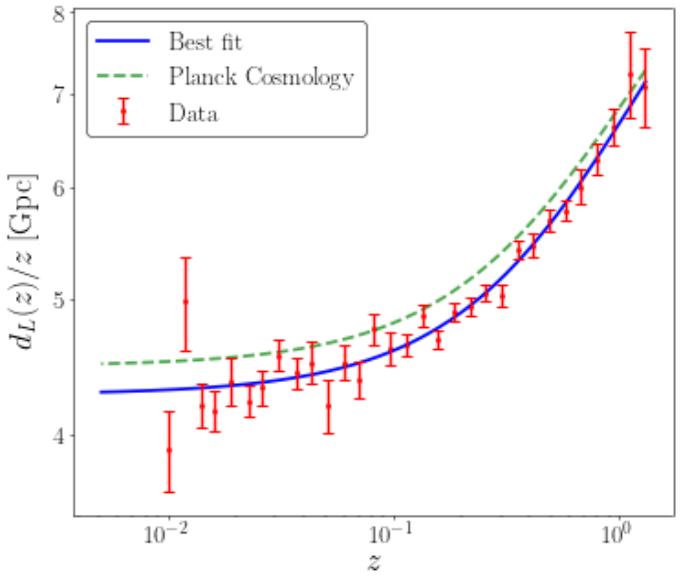

Fig. 9. The luminosity distance function obtained from the best fit values of C (blue line), compared with the result from the Planck cosmology (dashed green line), which is also shown in Fig. 6.

3. Milestone II

Having successfully implemented the background cosmology, the next step in developing our model is to include interactions between particles. After the Big Bang, the early universe was highly ionized. Due to Thompson scattering, photons were strongly coupled to baryons. As the Universe expanded, and the temperature dropped, neutral atoms were able to form, and the photons were able to escape from the plasma. These are the CMB photons we observe today. The period where neutral atoms formed is called recombination, and will be the main topic of this section. Our goal is to compute the number density of free electrons in the Universe, and use this to estimate when recombination occurred. The evolution of free electrons will affect both structure formation and the resulting power spectrum of the CMB photons, as we will study later.

We will use both the Saha and Peebles equation to compute the electron number density, and use this to compute the optical depth. From the optical depth, we will compute the so-called *visibility function*. In this section we will adapt natural units, where we set $c = \hbar = k_B = 1$. Additionally, we will make the assumption that Hydrogen is the only element present in the universe. Hence, we use $Y_p = 0$, rather than the value from Planck, given in Eq. (A.1), as we neglect Helium and heavier elements. Dodelson (2020)

The code for this milestone can be found on my GitHub repository: `https://github.com/Vikenes/AST5220/tree/main/projects/milestone2`

3.1. Theory

3.1.1. Optical depth and visibility function

A source that emits light with an intensity I_0 is attenuated by a factor $e^{-\tau(x)}$ as it travels through a medium, where τ is the optical depth of the medium. In the early universe we have $\tau \gg 1$, and the universe is said to be optically thick. As the universe expands and recombination takes place, the universe becomes optically thin, $\tau \ll 1$, and light is able to escape the primordial plasma and reach us. Considering Thompson scattering only, the optical depth is defined in terms of the scale factor, a, as (Callin 2006, Eq. (5))

$$\tau(\eta) = \int_{\eta}^{\eta_0} \mathrm{d}\eta' \, n_e \sigma_T a, \tag{33}$$

where n_e is the number density of free electrons,

$$\sigma_T = \frac{8\pi\alpha^2}{3m_e^2} = 6.6524587158 \cdot 10^{-29} \, \mathrm{m}^2 \tag{34}$$

is the Thompson cross-section and a is the scale factor. α is the fine-structure constant and m_e is the electron mass. Using Eq. (14), we can rewrite Eq. (33) as a differential equation

$$\frac{\mathrm{d}\tau}{\mathrm{d}x} = -\frac{n_e \sigma_T}{H}, \tag{35}$$

which we can solve numerically once we know n_e. The initial condition is $\tau(x = 0) = 0$, as the universe is transparent today.

From the optical depth, we obtain the so-called *visibility function* (Callin 2006, Eq. (8))

$$\tilde{g}(x) = -\tau' e^{-\tau}, \tag{36}$$

which is normalized as

$$\int_{-\infty}^{0} \mathrm{d}x\, \tilde{g}(x) = 1. \tag{37}$$

The normalization means that $\tilde{g}(x)$ is a probability distribution, and we may interpret it as the probability of an observed CMB photon today having experienced its last scattering at a time x. The visibility function is sharply peaked around the time when the photons decouple from the baryons, and is often referred to as the surface of last scattering. We may therefore use the peak of $\tilde{g}(x)$ to estimate the time when decoupling took place in the early universe.

3.1.2. Electron density

The final thing we need to compute τ and $\tilde{g}$ is the number density of free electrons. To compute the evolution of free electrons, we have to consider the Boltzmann equation (Dodelson 2020, Eq. (3.19))

$$\frac{\mathrm{d}f}{\mathrm{d}t} = C[f], \tag{38}$$

where f is the distribution function and $C[f]$ is a collision term.

We will not consider the full Boltzmann equation, but an approximated version relevant for the recombination. Following the notation and definitions from (Dodelson 2020, Eq. (4.5)-(4.9)), the equation we consider is given as

$$a^{-3}\frac{\mathrm{d}(n_1 a^3)}{\mathrm{d}t} = n_1^{(0)} n_2^{(0)} \langle \sigma v \rangle \left\{ \frac{n_3 n_4}{n_3^{(0)} n_4^{(0)}} - \frac{n_1 n_2}{n_1^{(0)} n_2^{(0)}} \right\}, \tag{39}$$

where n_i denotes the number density of a particle species i, with $n_i^{(0)}$ referring to its value in chemical equilibrium, and $\langle \sigma v \rangle$ is the thermally averaged cross-section. The only reaction we will consider for recombination is

$$e^- + p^+ \leftrightarrow H + \gamma. \tag{40}$$

For the photons we will assume $n_\gamma = n_\gamma^{(0)}$. From now on we use e and p as subscripts to denote free electrons and protons, respectively, and a subscript H to denote neutral Hydrogen.

Instead of computing n_e directly, we will compute the fractional electron density

$$X_e \equiv \frac{n_e}{n_e + n_H} \approx \frac{n_e}{n_b}, \tag{41}$$

where n_b is the total baryon density of the universe. Since the universe must be electrically neutral, we have $n_e = n_p$, and assuming no heavier elements than Hydrogen gives $n_b \approx n_p + n_H$. Neglecting the small mass difference between the proton and the Hydrogen, the baryon density can be written as

$$n_b \approx \frac{\rho_b}{m_H} = \frac{\Omega_{b0}\rho_{c0}}{m_H a^3}, \tag{42}$$

where $\rho_{c0} \equiv \frac{H_0^2}{8\pi G}$ is the critical density of the universe today and m_H is the Hydrogen mass.

Before recombination occurs, the interaction rates greatly exceed the expansion rate of the universe, and for Eq. (39) to be valid we must have that

$$\frac{n_e n_p}{n_H} = \frac{n_e^{(0)} n_p^{(0)}}{n_H^{(0)}}. \tag{43}$$

In terms of X_e, this reduces to the Saha equation

$$\frac{X_e^2}{1 - X_e} = \frac{1}{n_b}\left(\frac{m_e T_b}{2\pi}\right)^{3/2} e^{-\epsilon_0/T_b}, \tag{44}$$

where T_b is the temperature of the baryons, and ϵ_0 is the Hydrogen ionization energy. The time evolution of T_b is governed by a differential equation coupled to X_e. However, we will assume that it follows the photon temperature, T_γ, evolving as

$$T_b = T_\gamma = T_{\mathrm{CMB}0} e^{-x}. \tag{45}$$

At later times, Eq. (43) is no longer a valid approximation, and we have to solve Eq. (39). Additionally, we have to take processes related to atomic physics into account, so the differential equation we will consider is the Peebles equation

$$\frac{\mathrm{d}X_e}{\mathrm{d}x} = \frac{C_r(T_b)}{H}\left[\beta(T_b)(1 - X_e) - n_H \alpha^{(2)}(T_b) X_e^2\right], \tag{46}$$

where $C_r(T_b)$, $\beta(T_b)$ and $\alpha^{(2)}(T_b)$ are quantities related to interaction effects, and are given by

$$C_r(T_b) = \frac{\Lambda_{2s\to 1s} + \Lambda_\alpha}{\Lambda_{2s\to 1s} + \Lambda_\alpha + \beta^{(2)}(T_b)}, \tag{47a}$$

$$\Lambda_{2s\to 1s} = 8.227\ \mathrm{s}^{-1}, \tag{47b}$$

$$\Lambda_\alpha = H\frac{(3\epsilon_0)^3}{(8\pi)^2 n_{1s}}, \tag{47c}$$

$$n_{1s} = (1 - X_e) n_H, \tag{47d}$$

$$\beta^{(2)}(T_b) = \beta(T_b) e^{3\epsilon_0/4T_b}, \tag{47e}$$

$$\beta(T_b) = \alpha^{(2)}(T_b)\left(\frac{m_e T_b}{2\pi}\right)^{3/2} e^{-\epsilon_0/T_b}, \tag{47f}$$

$$\alpha^{(2)} = \frac{64\pi}{\sqrt{27\pi}}\frac{\alpha^2}{m_e^2}\sqrt{\frac{\epsilon_0}{T_b}}\phi_2(T_b), \tag{47g}$$

$$\phi_2(T_b) = 0.448 \ln(\epsilon_0/T_b). \tag{47h}$$

The main reason behind these additional equations is that Hydrogen production is inefficient at $T_b \simeq \epsilon_0$. Direct recombination to the Hydrogen ground state is likely to produce a photon with energy greater than ϵ_0, which will ionize another nearby Hydrogen atom, resulting in no net Hydrogen production. Recombination is achieved when an electron and proton combine to an excited Hydrogen atom, followed by the atom's decay into the ground state, which is a slow process.

In Sect. 3.2.2 we discuss how combine the Saha and Peebles equation to compute X_e.

3.1.3. Sound Horizon at decoupling

Before recombination happens, baryons and photons are tightly coupled. For this reason, the baryons and photons behave as if they were a single fluid, and the sound speed of this fluid is given by (Dodelson 2020, Eq. (9.21)) (where we use $R \to 1/R$)

$$c_s(x) = \frac{c}{\sqrt{3}}\sqrt{\frac{R(x)}{1+R(x)}}, \quad R(x) = \frac{4\Omega_\gamma(x)}{3\Omega_b(x)}. \tag{48}$$

The total co-moving distance a sound wave in this plasma could have travelled since the Big Bang is known as the sound-horizon, which is given as

$$s(x) = \int_{-\infty}^{x} \frac{\mathrm{d}x' c_s}{\mathcal{H}}. \tag{49}$$

From this we can compute the sound horizon at decoupling, $r_s = s(x_{\rm rec})$, which is an important quantity of the CMB. Thus, we have an additional ODE to solve,

$$\frac{\mathrm{d}s(x)}{\mathrm{d}x} = \frac{c_s}{\mathcal{H}}, \tag{50}$$

with $s(x_{\rm ini}) = \frac{c_s(x_{\rm ini})}{\mathcal{H}(x_{\rm ini})}$ as the initial condition, following the same reasoning as we did for $\eta'(x)$ in Eq. (15).

3.2. Implementation details

To compute X_e, we use the Saha equation initially, as it is a good approximation at early times when $X_e \approx 1$. This is also the regime where the Peebles equation is unstable, and we therefore consider the Saha equation for $X_e > X_e^{\rm tol}$. Once we reach $X_e < X_e^{\rm tol}$ we use the final value from the Saha equation as our initial condition to solve the Peebles equation. The Peebles equation is then used all the way to today, at $x = 0$. For this report, we choose $X_e^{\rm tol} = 0.99$. For comparison with the Saha equation alone, we set $X_e^{\rm tol} = 10^{-6}$. Once X_e is computed we get $n_e(x)$ from Eq. (41).

3.2.1. Solving the Saha Equation

Solving the Saha equation is done by solving a quadratic formula for X_e. At early times, however, the RHS of Eq. (44) will be enormous, and may cause numerical errors when solving the quadratic formula. To avoid this, we use the first order approximation $\sqrt{1+x} \approx 1 + \frac{x}{2}$ for $|x| \ll 1$ at early times. The Saha equation is thus implemented as

$$X_e = \begin{cases} 1, & y > 10^7, \\ \frac{y}{2}\left[-1 + \sqrt{1+4/y}\right], & y \le 10^7, \end{cases} \tag{51}$$

where y refers to the RHS of Eq. (44). Since X_e is strictly positive, we have omitted the negative solution. The exact value of 10^7 is chosen to ensure both $X_e \not> 1$, and $X_e \not< X_e^{\rm tol}$ when the quadratic formula is to be used.

3.2.2. Solving the Peebles Equation

To solve Eq. (46) numerically, we follow the same procedure as we did for $\eta(x)$, but for the initial condition we use the final value of X_e that we obtained from the Saha equation.

At late times, when the baryon temperature gets low, the exponent term in Eq. (47e) for $\beta^{(2)}(T_b)$ become sufficiently large to yield an overflow. However, this is also where $\beta(T_b) \to 0$, due to its exponential factor (Eq. (47f)). This exponential factor causes $\beta^{(2)}(T_b) \to 0$ at late times. To avoid overflow, we implement the equation for $\beta^{(2)}(T_b)$ as

$$\beta^{(2)}(T_b) = \begin{cases} 0, & \epsilon_0/T_b > 200, \\ \beta(T_b)e^{3\epsilon_0/4T_b}, & \epsilon_0/T_b \le 200. \end{cases} \tag{52}$$

3.2.3. Optical depth and visibility function

With n_e we can then solve Eq. (35) for $\tau(x)$ with the aforementioned initial condition of $\tau(x = 0) = 0$. We therefore integrate backwards, starting from $x = 0$. The visibility function is now easily obtained, as $\tau'(x)$ is given analytically by Eq. (35). From this, we get immediately $\tilde{g}(x)$.

We also need the second derivative of τ, as well as the first two derivatives of $\tilde{g}$. For $\tau''(x)$, we compute it from numerically differentiating the $\tau'(x)$ data. [1] We use this to compute

$$\tilde{g}'(x) = \left|\tau'(x)^2 - \tau''(x)\right| e^{-\tau(x)}, \tag{53}$$

and obtain $\tilde{g}''(x)$ by numerically differentiating $\tilde{g}'(x)$. This is done to avoid potential errors that may occur when numerically computing the second derivative of $\tilde{g}(x)$, if $\tilde{g}(x)$ is somewhat ill-behaved at certain times. [2]

3.2.4. Determining the time of recombination and decoupling

To estimate the times when recombination takes place, we define this as

$$X_e(x = x_{\rm recombination}) = 0.1, \tag{54}$$

where the value $X_e = 0.1$ is chosen arbitrarily.

For decoupling, we find $x_{\rm decoupling}$ as the point where $\tilde{g}'(x_{\rm decoupling}) = 0$. However, we limit the time values to $x \in [x_0 \pm 0.1]$, where x_0 is defined by $\tau(x_0) = 1$. This is done to avoid x values where $\tilde{g}(x) = 0$.

3.3. Results

3.3.1. Electron fraction

The evolution of the electron fraction with time is shown in Fig. 10. Here, we have included the solution obtained through the Saha equation alone for comparison. In the figure we also show the time periods when recombination occurs according to the two solutions, i.e. when $X_e = 0.1$. The time of decoupling has been omitted, since it is very close to the recombination time, as shown in table 2.

We see that the Peebles equation predicts the production of neutral Hydrogen to take much longer time than the Saha equation. Recombination therefore occurs at a much lower temperature than the binding energy of Hydrogen, as expected. Towards $x = 0$ the Peebles equation give $X_e \ll 1$, but we never reach $X_e = 0$ entirely. From our solution we find that the current value is $X_e(x = 0) \approx 2.026 \cdot 10^{-4}$. On the other hand, the Saha equation reaches $X_e = 0$ before $x = 0$ is reached, predicting now free electrons in the universe.

[1] Couldn't we just compute it analytically? I get a tiny "bump" in τ'' near $X_e^{\rm tol}$, and I don't know if this will cause problems later on, and therefore didn't want to spend too much time on it if wasn't needed.

[2] I don't know if this is useful, or helps, at all. I don't know if we care about the derivatives at x-values where this might be an issue.

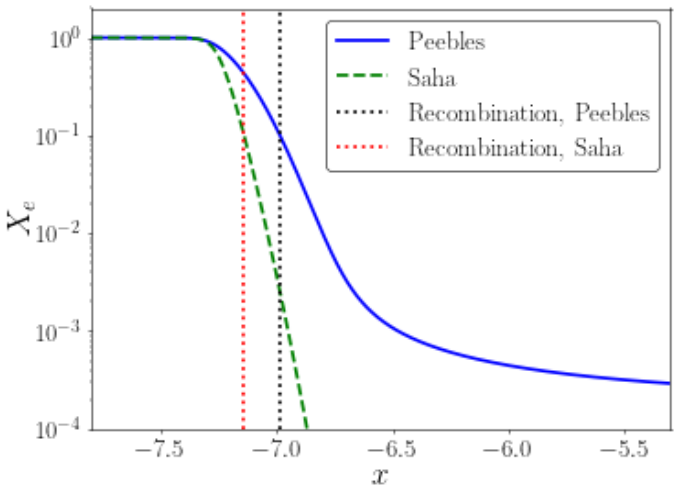

Fig. 10. Free electron fraction computed from the Saha equation only (dashed green curve) and from the Peebles equation (solid blue curve), where the Saha equation was used at early times, until $X_e < 0.99$. The recombination times is shown for both solutions.

3.3.2. Optical depth and visibility function

The optical depth, and its first two derivatives is shown in Fig. 11. We see that the three quantities rapidly drop by several orders of magnitude near $x = -7$, around the time of recombination. Looking at Fig. 12 we see that the rapidly varying optical depth results in a sharply peaked $\tilde{g}$.

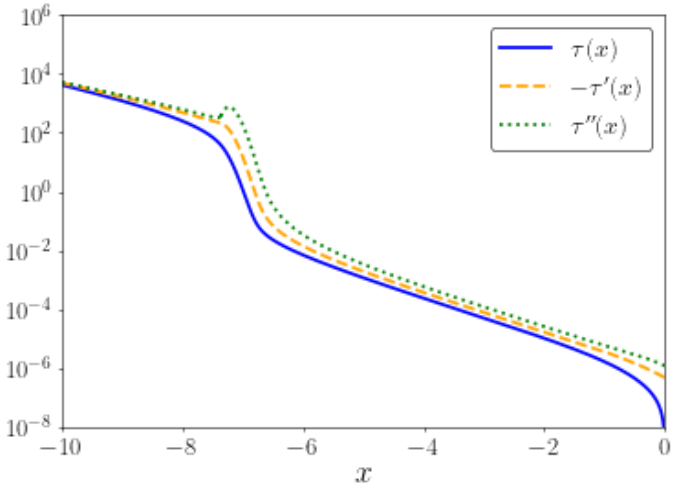

Fig. 11. The optical depth, $\tau(x)$ and its two first derivatives with respect to x.

3.3.3. Times of recombination and decoupling

The period of recombination and decoupling, as computed from the Peebles equation, is given in table 2. We see that the photons and baryons decouple later than recombination occurs, as is expected. This does depend on how we define the two periods, and is thus not a very conclusive result on its own. Using a higher value of X_e for instance would yield a larger separation between the two events.

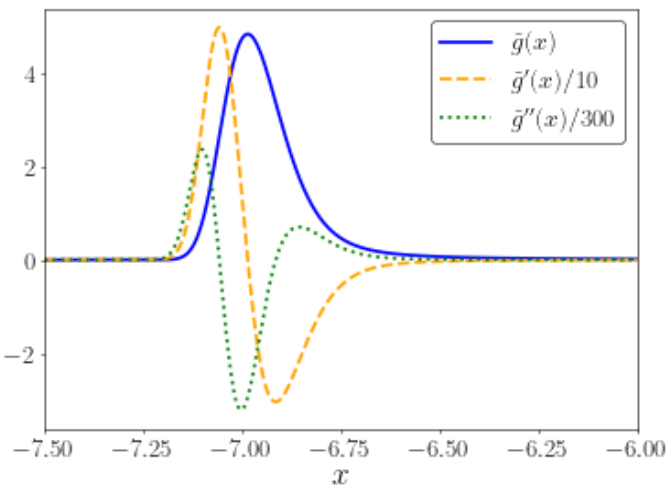

Fig. 12. The visibility function, $\tilde{g}(x)$ (solid curve), and its derivatives, $\tilde{g}'(x)/10$ (dashed curve) and $\tilde{g}''(x)/300$ (dotted curve). The derivatives have been scaled in order to view them all in the same plot.

Table 2. Times when decoupling and recombination occurs, computed from the Peebles equation.

Peebles	x	z	t [yr]	r_s [Mpc]
Decoupling	-6.98534	1079.7	377 782	145.3
Recombination	-6.98549	1079.8	377 690	

Table 3. Times when decoupling and recombination occurs, computed from the Saha equation.

Saha	x	z	t [yr]
Decoupling	-7.15485	1279.3	283 611
Recombination	-7.14035	1260.9	290 686

4. Milestone III

So far we have only considered the flat FLRW metric for a homogeneous Universe, and used this to study the recombination history of the Universe. In this section we will consider small perturbations to the background, and thereby introduce inhomogeneities. We will consider perturbations to the FLRW metric and the matter contents of the Universe, where we limit ourselves to photons, baryons and CDM (Check if CDM is declared). We will restrict ourselves to linear perturbations only, which allows us to derive good approximations for the Boltzmann and Einstein equations. From this we are able to study the evolution of structure in the early Universe, which we later will connect to statistical observables in the Universe.

The code for this milestone can be found on my GitHub repository: `https://github.com/Vikenes/AST5220/tree/main/projects/milestone3`

4.1. Theory

In this section we present the equations governing the evolution of the perturbed quantities. We will only present the relevant equations here, which are all obtained from Dodelson (2020) and Callin (2006), unless otherwise stated. We refer to Dodelson for a detailed derivation of the equations. For the notation, we adapt that of Callin.

4.1.1. Metric Perturbations

For the perturbed metric we consider the Newtonian gauge (Explain/cite), and write it as

$$g_{\mu\nu} = \begin{pmatrix} -(1+2\Psi) & 0 \\ 0 & a^2\delta_{ij}(1+2\Phi) \end{pmatrix}, \tag{55}$$

where we have introduced the scalar perturbations Ψ and Φ, which are functions of both position and time. For $\Psi = \Phi = 0$ we obtain the FLRW metric. Photon perturbations are defined in terms of the relative temperature variations, Θ, via

$$T(\boldsymbol{k}, \mu, \eta) = T^{(0)}(\eta)\left[1 + \Theta(\boldsymbol{k}, \mu, \eta)\right], \tag{56}$$

where $\boldsymbol{k}$ is the Fourier transformed variable corresponding to position $\boldsymbol{x}$, and $\mu \equiv \frac{\boldsymbol{k}\cdot\boldsymbol{p}}{kp}$. The temperature perturbations only depend on the photon momentum in terms of their directions, and we therefore expand Θ in terms of multipoles as

$$\Theta_\ell = \frac{i^\ell}{2}\int_{-1}^{1}\mathcal{P}_\ell(\mu)\Theta(\mu)\,\mathrm{d}\mu \Leftrightarrow \Theta(\mu) = \sum_{\ell=0}^{\infty}\frac{2\ell+1}{i^\ell}\Theta_\ell\mathcal{P}_\ell(\mu), \tag{57}$$

where $\mathcal{P}_\ell(\mu)$ are Legendre polynomials. The most important terms are the monopole, Θ_0, the dipole, Θ_1, and the quadrupole, Θ_2. The monopole is related to the density perturbation of photons, $\delta_\gamma = 4\Theta_0$, and the dipole to the photon velocity, $v_\gamma = -3\Theta_1$. These terms represent the average background temperature, and the temperature fluctuation due to Doppler effects, respectively Check last sentence.

For CDM we denote the density and velocity perturbations as δ_{CDM} and v_{CDM}, respectively, and similarly denote the baryon perturbations as δ_b and v_b.

Fix structure afterwards.

4.1.2. Perturbation equations

Having introduced the perturbed quantities of interest, the system of ODEs, given in Fourier space, that we will solve are given by (Callin 2006, Eq. (22))

$$\Theta_0' = -\frac{k}{\mathcal{H}}\Theta_1 - \Phi', \tag{58a}$$

$$\Theta_1' = \frac{k}{3\mathcal{H}}\Theta_0 - \frac{2k}{3\mathcal{H}}\Theta_2 + \frac{k}{3\mathcal{H}}\Psi + \tau'\left[\Theta_1 + \frac{1}{3}v_b\right], \tag{58b}$$

$$\Theta_\ell' = \frac{\ell k}{(2\ell+1)\mathcal{H}}\Theta_{\ell-1} - \frac{(\ell+1)k}{(2\ell+1)\mathcal{H}}\Theta_{\ell+1} + \tau'\left[\Theta_\ell - \frac{1}{10}\Pi\delta_{\ell,2}\right], \quad 2 \le \ell < \ell_{\max}, \tag{58c}$$

$$\Theta_\ell' = \frac{k}{\mathcal{H}}\Theta_{\ell-1} - c\frac{(\ell+1)}{\mathcal{H}\eta(x)}\Theta_\ell + \tau'\Theta_\ell, \quad \ell = \ell_{\max}, \tag{58d}$$

$$\delta_{\mathrm{CDM}}' = \frac{k}{\mathcal{H}}v_{\mathrm{CDM}} - 3\Phi', \tag{58e}$$

$$v_{\mathrm{CDM}}' = -v_{\mathrm{CDM}}\frac{k}{\mathcal{H}}\Psi, \tag{58f}$$

$$\delta_b' = \frac{k}{\mathcal{H}}v_b - 3\Phi', \tag{58g}$$

$$v_b' = -v_b - \frac{k}{\mathcal{H}}\Psi + \tau' R(3\Theta_1 + v_b), \tag{58h}$$

$$\Phi' = -\Psi - \frac{k^2}{3\mathcal{H}^2}\Phi + \frac{H_0^2}{2\mathcal{H}^2}[\Omega_{\mathrm{CDM}0}a^{-1}\delta_{\mathrm{CDM}} + \Omega_{b0}a^{-1}\delta_b + 4\Omega_{\gamma 0}a^{-2}\Theta_0], \tag{58i}$$

$$\Psi = -\Phi - \frac{12H_0^2}{k^2a^2}\Omega_{\gamma 0}\Theta_2. \tag{58j}$$

Compared to (Callin 2006, Eq. (22)), we have set all terms involving $\Theta_{P\ell}$ and $\mathcal{N}$ to zero, as we neglect polarization and neutrinos. Thus, we have $\Pi = \Theta_2$.

Eq. (58d) comes from (Callin 2006, Eq. (49)). In Sect. 4.1.4 we discuss how we can compute any Θ_ℓ from Θ_0 and Θ_2. Due to the recursive expression for Θ_ℓ' we need higher moments to compute Θ_2 accurately. Truncating the series by setting $\Theta_{\ell_{\max}} = 0$ would lead to numerical errors propagating down to Θ_2. The expression for $\Theta_{\ell_{\max}}$ comes from assuming $\Theta_\ell(k,\eta) \sim j_\ell(k\eta)$ at high ℓ, together with the recursive relation of $j_\ell(k\eta)$.

The equation for Ψ is an algebraic equation, and its value is inserted in the other equations. Noting that Φ' is the only derivative of a perturbed quantity found on the RHS of Eqs. (58), we solve for it first, and insert this value into the other equations. At early times, τ' is very large, as seen from Fig. 11. Since we're considering small perturbations, this implies that terms multiplied with τ' should be set to zero in Eq. (58). This is referred to as the *Tight coupling regime*, where the equations we have to solve are slightly modified. There are also changes that have to be made due to numerical stability at early times. We therefore proceed with the discussion of initial conditions in Sect. 4.2.

4.1.3. Initial conditions

For the initial conditions we follow Winther (2023), with $f_\nu = 0$ as we omit neutrinos[3]. The set of ODEs we solve are linear, so we can choose a particular normalization, which we adjust for when computing the Power spectrum later on. The initial condi-

[3] Note that Winther has a sign error in his expression for Ψ

tions are

$$\Psi = -\frac{2}{3}, \tag{59a}$$
$$\Phi = -\Psi, \tag{59b}$$
$$\delta_{\mathrm{CDM}} = \delta_b = -\frac{3}{2}\Psi, \tag{59c}$$
$$v_{\mathrm{CDM}} = v_b = -\frac{k}{2\mathcal{H}}\Psi, \tag{59d}$$
$$\Theta_0 = -\frac{1}{2}\Psi, \tag{59e}$$
$$\Theta_1 = \frac{k}{6\mathcal{H}}\Psi, \tag{59f}$$
$$\Theta_2 = -\frac{20k}{45\mathcal{H}\tau'}\Theta_1, \tag{59g}$$
$$\Theta_\ell = -\frac{\ell}{2\ell+1}\frac{k}{\mathcal{H}\tau'}\Theta_{\ell-1}. \tag{59h}$$

The expressions for Θ_ℓ for $\ell > 1$ comes from the fact that τ' is very large at early times, which we discuss in the next subsection.

4.1.4. Line-of-sight integration

From Eq. (58c) we see that we have to solve a huge system of ODEs if we want to probe the CMB to scales around $\ell \sim 1000$. However, by exploiting the LOS-integration technique (Cite), Θ_ℓ can be obtained from computing the integral

$$\Theta_\ell(k, x=0) = \int_{-\infty}^{0} \tilde{S}(k,x) j_\ell[k(\eta_0 - \eta(x))]\,\mathrm{d}x, \tag{60}$$

where $\tilde{S}(k,x)$ is the source function, and is given by

$$\tilde{S}(k,x) = \tilde{g}\left[\Theta_0 + \Psi + \frac{1}{4}\Pi\right] + e^{-\tau}\left[\Psi' - \Phi'\right] - \frac{1}{k}\frac{\mathrm{d}}{\mathrm{d}x}(\mathcal{H}\tilde{g}v_b) + \frac{3}{4k^2}\frac{\mathrm{d}}{\mathrm{d}x}\left[\mathcal{H}\frac{\mathrm{d}}{\mathrm{d}x}(\mathcal{H}\tilde{g}\Pi)\right]. \tag{61}$$

Since we have $\Pi = \Theta_2$, the highest photon multipole required to compute any multipole Θ_ℓ from Eq. (60) is Θ_2. Thus, the number of multipole we have to compute from the coupled ODEs in Eq. (58) is governed by the value of ℓ_{max} which ensures sufficient accuracy in Θ_2. This is explained more thoroughly in Section

4.2. Implementation details

4.2.1. Tight coupling regime

During tight coupling, Eq. (62c) becomes numerically unstable, since the last term consists of multiplying τ' with $\Theta_1 + v_b/3$, where τ' is huge, and the latter term is approximately 0. We therefore have to resort to a numerically stable equation for $\Theta_1 + v_b$. Following Callin, the tight coupling regime is computed with

$$\varrho q = -\left[(1-R)\tau' + (1+R)\tau''\right](3\Theta_1 + v_b) - \frac{k}{\mathcal{H}}\Psi + (1 - \frac{\mathcal{H}'}{\mathcal{H}})\frac{k}{\mathcal{H}}(-\Theta_0 + 2\Theta_2) - \frac{k}{\mathcal{H}}\Theta_0', \tag{62a}$$
$$v_b' = \frac{1}{1+R}\left[-v_b - \frac{k}{\mathcal{H}}\Psi + R(q + \frac{k}{\mathcal{H}}[-\Theta_0 + 2\Theta_2 - \Psi])\right], \tag{62b}$$
$$\Theta_1' = \frac{1}{3}(q - v_b'), \tag{62c}$$

where we introduced the parameter

$$\varrho = (1+R)\tau' + \frac{\mathcal{H}'}{\mathcal{H}} - 1. \tag{63}$$

In the tight coupling regime we use the initial conditions given in Eq. (59). We then solve the ODEs given in Eq. (58), but compute Θ_1' and v_b' in the end by using Eq. (62). In this regime we use Eqs. Eq. (59g) and (59h) for Θ_2 and Θ_ℓ, respectively, as we assume $\Theta_\ell' = 0$ for $\ell > 2$ Check this.

Next, we need to determine when the tight coupling approximation is valid. We use the same conditions as Callin, namely that the approximation holds as long as $|\tau'| > 10$ and $|k/\mathcal{H}\tau'| < 1/10$, and that it should not be used after the start of recombination. For the last condition, we choose $x < -8.3$ as the time when recombination starts. If any of these three conditions fails, we switch to the full ODEs. We then use the final results from the tight coupling regime as initial conditions for the ODEs in Eq. (58), and integrate up to $x = 0$.

4.2.2. Integration details (working title)

Write about details regarding integration

When solving the perturbation ODEs we integrate across x for each mode k, where we choose a logarithmic spacing for the k values.

4.2.3. Source function

For the source function, we use values of k distributed quadratically (explain why) as

$$k_i = k_{\mathrm{min}} + (k_{\mathrm{max}} - k_{\mathrm{min}})(i/N_k)^2, \tag{64}$$

where we use $N_k = 100$ value of k (Check this).

4.3. Results

In this section we present plots showing the evolution of some perturbation quantities. In Figs. 13-19 we indicate the time when tight coupling end by a dotted black vertical line. The modes we have chosen to include in these results are $k = \{0.001\mathrm{Mpc}, 0.01\mathrm{Mpc}, 0.1\mathrm{Mpc}\}$.

4.3.1. Matter perturbations

We begin by plotting the velocity and density evolution for the matter components, shown in Fig. 13 and 14, respectively. In both figures, we see that the baryons and CDM follow each other initially, before recombination starts. During recombination, we see that the baryons deviate from the CDM on small scales. This is expected, as pressure from photons will counteract the gravitational collapse of baryons on small scales initially. As the baryon density drops they cool and collapse back in again, until the photons push them out again. This causes the oscillating features seen in both figures.

As we approach $x = -6$, the Universe is mostly neutral, as seen from Fig. 10, and baryons are able to fall freely into the CDM potential wells, and we therefore have $\delta_{\mathrm{CDM}} \sim \delta_b$ during later times.

For the larger scales, CDM collapses much later. At this point the Universe is already transparent, so baryons simply follow the CDM without oscillating.

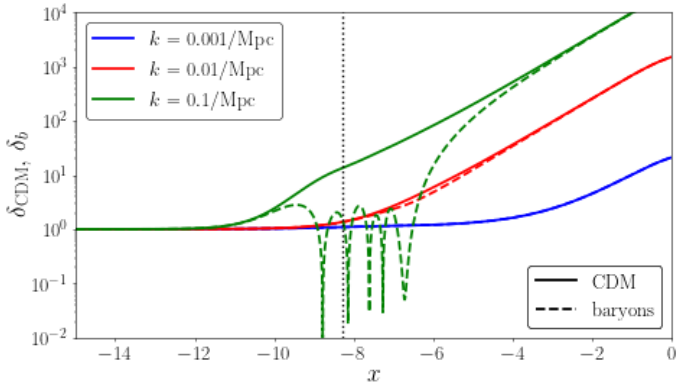

Fig. 13. Time evolution of $\delta_{\rm CDM}$ (solid line) and δ_b (dashed line) for three different modes. Long before and long after recombination, the two species follow each other closely. Around the epoch of recombination we see large fluctuations for the baryons, particularly for the highest k-mode, i.e. the smallest scales.

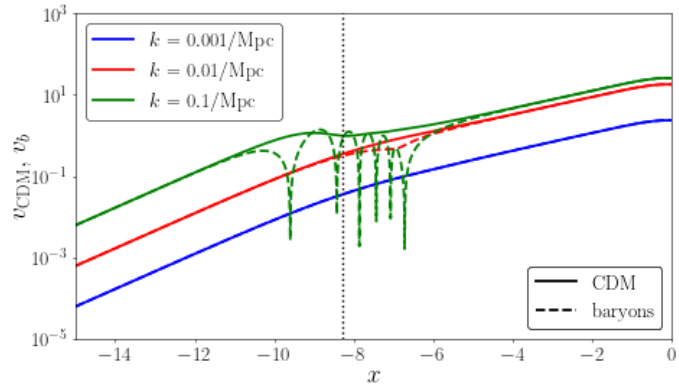

Fig. 14. Evolution of $v_{\rm CDM}$ (solid line) and v_b (dashed line) for three different modes. The most evident deviation between the baryons and CDM is for the largest mode.

For the velocities, we see a similar behaviour between the baryons and CDM as we did for the density. Write more here later

Maybe I should plot baryons and photons together

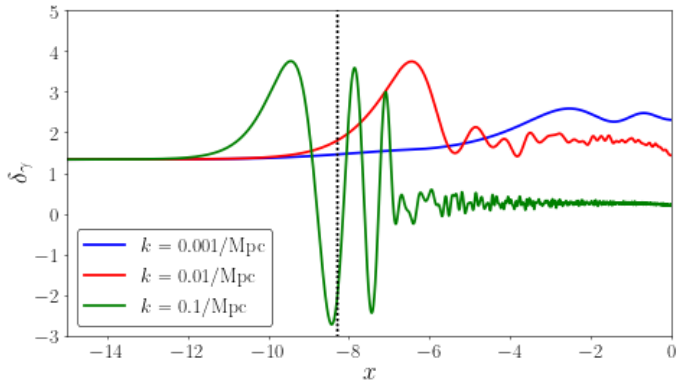

Fig. 15. Time evolution of δ_γ for three different modes.

4.3.2. Metric perturbations

The evolution of Φ is shown in Fig. 17.

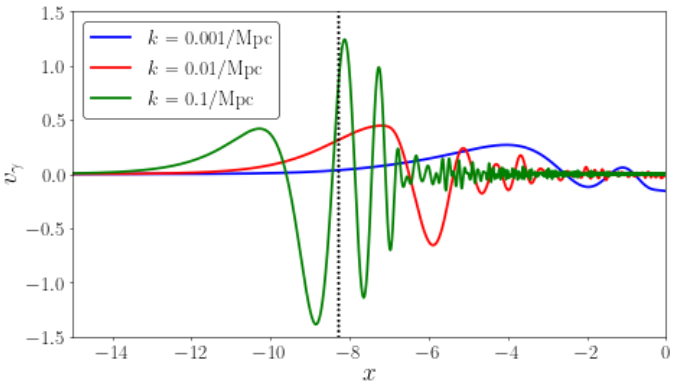

Fig. 16. Evolution of v_γ.

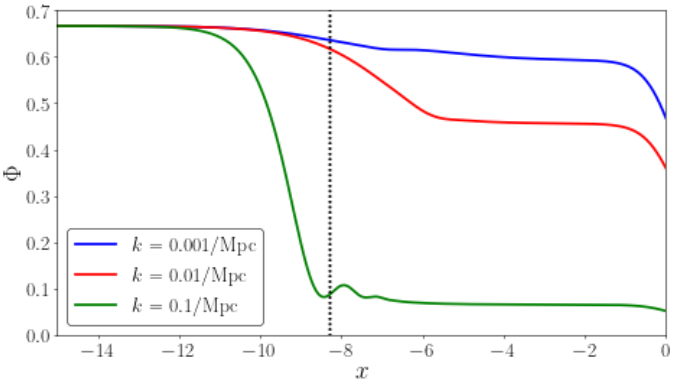

Fig. 17. Evolution of Φ.

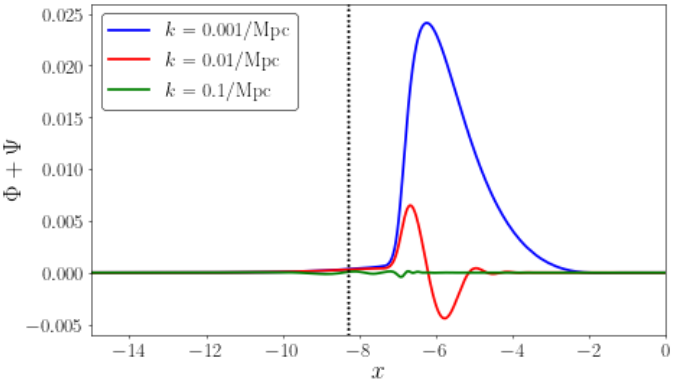

Fig. 18. Evolution of the combined metric perturbations, $\Phi + \Psi$

5. Milestone IV

Some introduction about what it is all about.

5.1. Theory

The theory behind this milestone.

5.2. Implementation details

Something about the numerical work.

5.3. Results

Show and discuss the results.

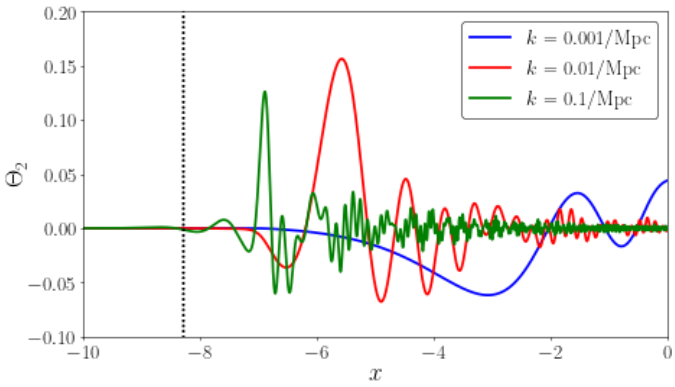

Fig. 19. Evolution of the quadrupole, Θ_2. At $x < -10$, there is no apparent contribution of this quantity.

6. Conclusions

Write a short summary and conclusion in the end.

Acknowledgements. I thank my mom for financial support!

References

Betoule, M., Kessler, R., Guy, J., et al. 2014, A&A, 568, A22, doi: 10.1051/0004-6361/201423413
Callin, P. 2006, arXiv e-prints, astro, doi: 10.48550/arXiv.astro-ph/0606683
Dodelson, S. 2020, Modern Cosmology (Academic Press), doi: 10.1016/C2017-0-01943-2
Galassi, M. e. a. 2009, GNU scientific library reference manual (Network Theory Ltd.)
Planck Collaboration, Aghanim, N., Akrami, Y., et al. 2020, A&A, 641, A6, doi: 10.1051/0004-6361/201833910
Winther, H. A. 2023, Cosmology II: Initial conditions. https://cmb.wintherscoming.no/theory_initial.php#init

Appendix A: Fiducial parameters

The parameter values we use in this report are

$$
\begin{aligned}
h &= 0.67, \\
T_{\mathrm{CMB0}} &= 2.7255\,\mathrm{K}, \\
N_{\mathrm{eff}} &= 3.046, \\
\Omega_{b0} &= 0.05, \\
\Omega_{\mathrm{CDM0}} &= 0.267, \\
\Omega_{k0} &= 0, \\
\Omega_{\nu 0} &= N_{\mathrm{eff}} \cdot \frac{7}{8}\left(\frac{4}{11}\right)^{4/3} \Omega_{\gamma 0}, \\
\Omega_{\Lambda 0} &= 1 - (\Omega_{k0} + \Omega_{b0} + \Omega_{\mathrm{CDM0}} + \Omega_{\gamma 0} + \Omega_{\nu 0}), \\
n_s &= 0.965, \\
A_s &= 2.1 \cdot 10^{-9}, \\
Y_p &= 0.245, \\
z_{\mathrm{reion}} &= 8, \\
\Delta z_{\mathrm{reion}} &= 0.5, \\
z_{\mathrm{Hereion}} &= 3.5, \\
\Delta z_{\mathrm{Hereion}} &= 0.5,
\end{aligned}
\tag{A.1}
$$